FREIA Report 2014/02
February 2014

UPPSALA UNIVERSITET

DEPARTMENT OF PHYSICS AND ASTRONOMY
UPPSALA UNIVERSITY

Effects of emittance and energy spread in an electron bunch on THz radiation generated by a super-radiant source:

report III of the series of reports by the Swedish FEL Center

R. Chulkov[a], *V.A. Goryashko*[b], *V. Zhaunerchyk*[b,c]

[a] B.I. Stepanov Institute of Physics, National Academy of Science of Belarus, Nesalezhnasti Ave. 68, 220072 Minsk, Belarus
[b] Department of Physics and Astronomy, Uppsala University, Sweden
[c] Department of Physics, University of Gothenburg, Sweden

Department of
Physics and Astronomy
Uppsala University
P.O. Box 516
SE – 751 20 Uppsala
Sweden

Papers in the FREIA Report Series are published on internet in PDF- formats.
Download from http://uu.diva-portal.org

Effects of emittance and energy spread in an electron bunch on THz radiation generated by a super-radiant source

February 28, 2014

Ruslan Chulkov[a], Vitaliy Goryashko[b], Vitali Zhaunerchyk[b],[c]

[a]B.I. Stepanov Institute of Physics, National Academy of Science of Belarus, Nesalezhnasti Ave. 68, 220072 Minsk, Belarus

[b]Department of Physics and Astronomy, Uppsala University, Uppsala, Sweden

[c]Department of Physics, University of Gothenburg, Sweden

emails: r.chulkov@mail.ru; vitali.zhaunerchyk@physics.uu.se

February 28, 2014

Abstract

In this report we summarize our results on simulation of a super-radiant source operating at the THz spectral range. We consider an open-type undulator comprising plane magnets but without any guiding structure for generated THz field. The undulator is assumed to be driven by electron bunches of femtosecond duration which are produced by an rf Linac. Using a numerical model developed, we analyze effects of the bunch parameters on output performance of the super-radiant source and reveal some surprising results. Specifically, we show that degradation in bunch spatial quality (increase in the bunch emittance) should lead to decrease in angular divergence and spectral narrowing of the THz radiation. We also demonstrate that electron energy spread which commonly leads to bunch broadening and radiative energy drop can be eventually suppressed under appropriate conditions.

1 Introduction

Free Electron Lasers (FELs) are powerful versatile light sources in which the coherent light is emitted by free relativistic electrons propagating through a periodic magnetic field created by an undulator. Physical principles of FELs allow one to use them for generation of radiation in spectral regions extending from hard X-rays to far infra-red

(FIR). In the FIR or THz frequency range, FELs enable generation of tunable THz light in both continuous-wave and pulsed regimes.

Pulsed THz FELs are typically driven by radio-frequency linear accelerators (rf Linacs) which produce intense electron bunches with a duration lying in the picosecond or even in femtosecond range. Under sub-picosecond and femtosecond bunch excitation, wavelength of THz radiation gets comparable to or greater than the bunch length thereby enabling realizing the super-radiant operating regime of the FEL. In this case, FEL output intensity scales as squared number rather than number of electrons as it occurs in a SASE (self-amplified spontaneous emission) FEL. Thus, the super-radiant operating regime potentially proposes realization of a relatively compact THz FEL facility. Specifically, FEL interaction geometry can be a simple single-pass source without any optical feedback. Operation efficiency of such a source is strongly affected by parameters of driving electron bunch. Some of these parameter effects can be estimated analytically. However, more accurate approach requires direct numerical modeling which should takes into account general statistical properties of the electron bunches.

In this paper we present results of such modeling for a super-radiant single-pass THz source comprising an undulator with plane magnets. We focus on an open-type interaction geometry without any guiding structure for generated THz field. Below we briefly describe our numerical code which considers nonzero bunch emittance and electron energy spread and enables 3D modeling FEL dynamics when electron bunches are comparable to or shorter than the FEL resonant wavelength.

2 The Model

A key concept of the model is expanding the time-dependent THz field into a complete set of mutually orthogonal modes $\Psi_{m,n}$

$$E\left(\vec{r},t\right)=2\mathrm{Re}\Big\{\sum_{m,n}\int_0^\infty C_{m,n}\Psi_{m,n}e^{i\omega t-ik_z z}d\omega\Big\}, \tag{1}$$

$$H\left(\vec{r},t\right)=2\mathrm{Re}\Big\{\sum_{m,n}\int_0^\infty \frac{k_z}{\omega\mu_0}\,C_{m,n}\Psi_{m,n}e^{i\omega t-ik_z z}d\omega\Big\}. \tag{2}$$

Details of the concept can be found in Refs. [1, 2, 3, 4, 5]. In our model we used the Hermite-Gaussian modes which in the scalar notation have the form:

$$\Psi_{m,n}(x,y,z)=N_{n,m}H_m\left(\sqrt{2}\frac{x}{w(z)}\right)H_n\left(\sqrt{2}\frac{y}{w(z)}\right) \times\exp\left[-\frac{x^2+y^2}{w(z)^2}-ik_z\frac{x^2+y^2}{2\rho_c(z)}+i\psi_{m,n}(z)\right], \tag{3}$$

where $\vec{r}$ refers to the Cartesian coordinates with z and x,y being the longitudinal and the transverse coordinates, respectively, $C_{m,n}\left(z,\omega\right)$ are the slowly varying Fourier amplitudes of $\Psi_{m,n}(\vec{r})$ modes along z-direction, H_m and H_n are the Hermite polynomials of the m^{th}

and n^{th}-order, respectively, ω is the angular frequency, and c is the light velocity in vacuum, $k_z(\omega) = \omega/c$ is the propagation constant, and

$$N_{n,m}(z) = \frac{1}{w(z)} \left(\frac{2}{2^m 2^n m! n! \pi} \right)^{1/2} \tag{4}$$

is the normalizing factor so that

$$\int |\Psi_{m,n}|^2 \, d\vec{r} = 1. \tag{5}$$

The $\Psi_{m,n}$ modes possess two mutually orthogonal polarizations. Since for an undulator with linear magnets electrons wiggle predominantly perpendicular to the undulator magnetic field, only the x-polarization for which the direction of electric field nearly coincides with the wiggling motion of electrons, is considered in the model. In Eq. (3), (4), $w(z)$ is the mode spot size, $\rho_c(z)$ is the curvature radius of the wavefront, and $\psi_{m,n}(z)$ is the Guoy phase shift. $w(z)$, $\rho_c(z)$, and $\psi_{m,n}(z)$ are related to each other as follows:

$$w(z) = w_0 \sqrt{1 + \left(\frac{z}{z_R} \right)^2}, \quad w_0 = \sqrt{\frac{2z_R}{k_z}} \tag{6}$$

$$\rho_c(z) = z + \frac{z_R^2}{z}, \tag{7}$$

$$\psi_{m,n}(z) = (m + n + 1) \tan^{-1} \left(\frac{z}{z_R} \right), \tag{8}$$

where z_R is the Rayleigh length and w_0 is the mode spot size at the waist.

Inserting (3) into the inhomogeneous wave equation with source current $J(\vec{r}, w)$

$$\Delta E + k^2 E = -i\omega\mu_0 J, \tag{9}$$

and taking into account the fact that the Hermite-Gaussian modes are solutions of the free-space paraxial wave equation

$$\Delta_{\vec{r}} \Psi_{m,n} = 2ik_z \frac{\partial \Psi_{m,n}}{\partial z} \tag{10}$$

we get following equation for the mode amplitudes $C_{m,n}$

$$\frac{\partial C_{m,n}(\omega, z)}{\partial z} = \frac{\omega\mu_0}{2k_z} \exp(ik_z z) \int J(\vec{r}, \omega) \, \Psi^*_{m,n}(\vec{r}) \, d\vec{r}, \tag{11}$$

where

$$J(\vec{r}, \omega) = 2 \int J(\vec{r}, t) \exp(-i\omega t) \, dt = \\ - 2 \sum_j q_j \frac{\vec{v_j}}{v_{zj}} \delta(x - x_j) \, \delta(y - y_j) \exp(-i\omega t_j), \tag{12}$$

is determined only for positive frequencies $j = 1, .., N_p$ and q_j are the number and charge of the macroparticle, respectively, $\vec{v_j}$ and v_{zj} are the macroparticle velocity and its projection on z-axis.

For a linear undulator with plane magnets, only y-component of the magnetic field is considered. If macroparticle energy is high enough that $1/\gamma_j << 1$, where the macroparticle's Lorentz factor, and $k_u\gamma_j << 1$ for all z along the undulator, where $k_u = 2\pi/\lambda_u$ is the undulator wavenumber and λ_u is the undulator period, then wiggle-averaged macroparticle's trajectories can be derived analytically [6]. Equations for the averaged velocity components of the macroparticle can be written in the forms [7]:

$$v_{xj} \approx v_{0xj} - \sqrt{2}\frac{\theta_j A}{k_u}\left(1 + \frac{k_u^2 y_j^2}{2}\right), \tag{13}$$

$$v_{yj} \approx v_{0yj} + \theta_j y_{0j}\sin\left(\frac{c}{v_{zj}}\omega_{\beta j} z\right), \tag{14}$$

$$v_{zj} = \left[c^2\left(1 - \gamma_j^{-2}\right) - v_{xj}^2 - v_{yj}^2\right]^{\frac{1}{2}}, \tag{15}$$

where

$$\omega_{\beta j} = \frac{|e|\, cB_u}{\sqrt{2}m_e c^2 \gamma_j} \tag{16}$$

is the betatron frequency,

$$A = a_u\cos\left(k_u z\right) + b_u, \tag{17}$$

B_u is the magnetic flux density, e and m_e are the electron charge and mass, respectively, subscript "0" denotes variable values at the undulator entrance, and constants

$$[a_u, b_u] = \begin{cases} \left[\frac{1}{4}, -\frac{1}{4}\right], & z < \frac{\lambda_u}{2} \text{ or} \\ & \left(N_u - \frac{1}{2}\right)\lambda_u \le z < N_u\lambda_u \\ \left[\frac{3}{4}, \frac{1}{4}\right], & \frac{\lambda_u}{2} \le z < \lambda_u \text{ or} \\ & \left(N_u - 1\right)\lambda_u \le z < \left(N_u - \frac{1}{2}\right)\lambda_u \\ [1, 0], & \lambda_u \le z < \left(N_u - 1\right)\lambda_u \end{cases} \tag{18}$$

determine adiabatic input-output of the undulator[8]. Eqs. (13), (14), (15) should be used with equation for the Lorentz factor of the macroparticle γ_j [2]

$$\frac{\partial\gamma_j}{\partial z} = -\frac{e}{m_e c^2}\frac{v_{xj}}{v_{zj}}E_x\left(\vec{v_j}, t_j\right) \tag{19}$$

to calculate the average macroparticle trajectory.

In the model, we assume that the input electron bunch possesses the axial symmetry relative to z-direction and its waist locates at the undulator center for the ballistic electron propagation. Under specified above conditions, initial rms width $\sigma_{x,y}$ of the bunch is [9]:

$$\sigma_{x,y} = \sqrt{\frac{\epsilon}{4}\left(\beta_0 + \frac{L_u^2}{4\beta_0}\right)}, \tag{20}$$

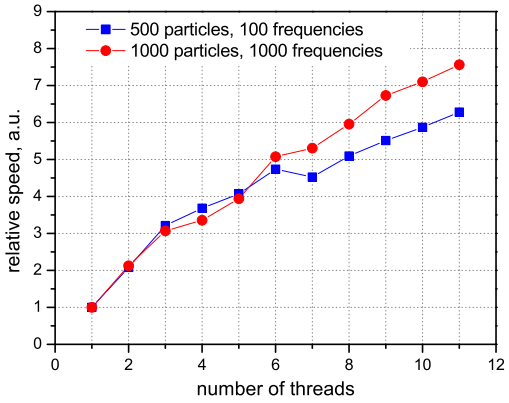

Figure 1: (Color online) Calculation speed as the function of number of processor's threads shown for two numerical tasks with different numbers of frequencies and macroparticles. The speed values are normalized to the single-thread speed.

where ϵ is the rms bunch emittance, β_0 is the geometrical β-function which determines the bunch waist length, and L_u is the undulator length. We used Gaussian statistics to simulate initial macroparticle distribution $[x_{0j}, y_{0j}]$ in the bunch along transverse directions. Their initial transverse velocities $[v_{0xj}, v_{0yj}]$ have been found according to the relations [10, 11]:

$$v_{0xj} = -\vartheta x_{0j} v_{0zj}, \quad v_{0yj} = -\vartheta y_{0j} v_{0zj}, \tag{21}$$

$$\vartheta = \frac{1}{\beta_0}\left(\frac{z_0}{\beta_0} + \frac{\beta_0}{z_0}\right)^{-1}. \tag{22}$$

We used the normal distribution for initial longitudinal macroparticle velocities v_{0zj} which are taken according to given values of energy spread and initial averaged energy E_e of electrons in the bunch. The numerical code has been implemented with the double-precision arithmetic. The finite-difference integration scheme on z was the 4-th order Bashforth-Moulton predictor-corrector with relative tolerance control on each z-step. Eq. (11) was integrated in frequency domain and Eq. (19) was in time domain. Mutual relations between time and frequency domains were realized via the Fourier transform. A typical calculation task requires 10^3 macroparticles, 10^3 steps on z, discretization by over $100 - 200$ frequencies, and at least $N_{max} = 200$ modes in the field decomposition.

FEL simulations have been done on HP Z420 multiprocessing workstation (3 x Intel Xeon 3.2GHz, 16GB RAM, Windows 7 64bit,) employing Microsoft Visual C++ platform. Multithreads OpenMP library has been used to parallelize the code. Fig. 1 demonstrates code performance as the function of number of processor threads loaded N_{thr}. As is seen, the gain in calculation speed grows linear with N_{thr} increase at the beginning and starts to slow down when $N_{thr>}3$. The cause of the gain saturation is sequential code sections and definite time needed for threads to synchronize and exchange by the data. For $N_{thr} = 10$, parallelization gives the $6 - 7$-th times growth in the calculation speed and results in decreasing the calculation time of a typical task down to an hour or less.

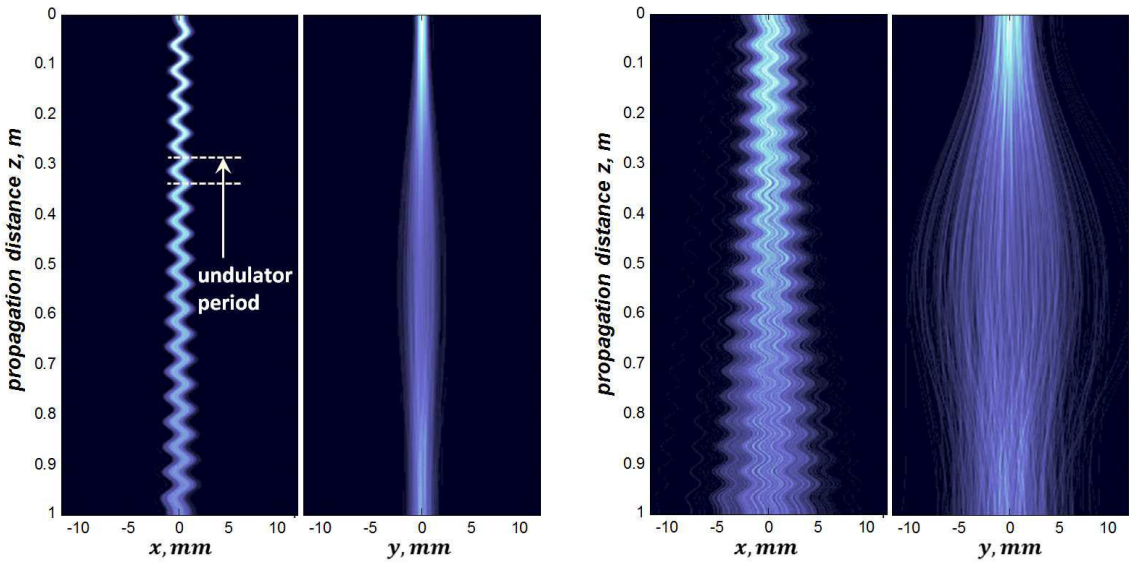

(a) ϵ_n =16 mm·mrad (b) ϵ_n =256 mm·mrad

Figure 2: (Color online) The macroparticle trajectories inside an undulator with L_u =1 m and λ_u =5.5 cm calculated for two different ϵ_n values when β_0 =3 m and E_x was taken to be zero.

3 Results and Discussion

Fig. 2 shows trajectories of the macroparticles inside an undulator calculated for two different values of normalized emittance $\epsilon_n = \gamma_0\epsilon$, 16 and 256 mm·mrad and geometrical β-function β_0 =3 m. For both the cases presented, we set $E_x = 0$ in Eq. (19) to be sure that only the bunch emittance would effect on the macroparticle trajectories. As is seen, increase in ϵ_n leads to considerable broadening of the bunch in both x and y directions. Wiggling motion of the particles are observed only in horizontal plane which is orthogonal to direction of undulator magnetic field whereas in vertical plane bunch slowly "breezes". Such breezing behavior is related to the betatron oscillations [10]. Note, that the betatron oscillations wash out a waist of the electron bunch which should be located at the undulator center for the ballistic electron transport.

Table 1: Parameters of simulation. The resonant frequency is 0.3 THz.

Bunch charge, Q_b	1 nC
Mean electron energy, E_e	9.0 MeV
Bunch duration, τ_b	150 fs (rms)
Bunch β_0-function	3.0 m
Magnetic flux density, B_u	0.311 T
Undulator period, λ_u	11 cm
Number of periods, N_u	9
Undulator parameter, K_u	2.26

Fig. 3a shows output energy E_{THz} of the THz pulse calculated as a function of

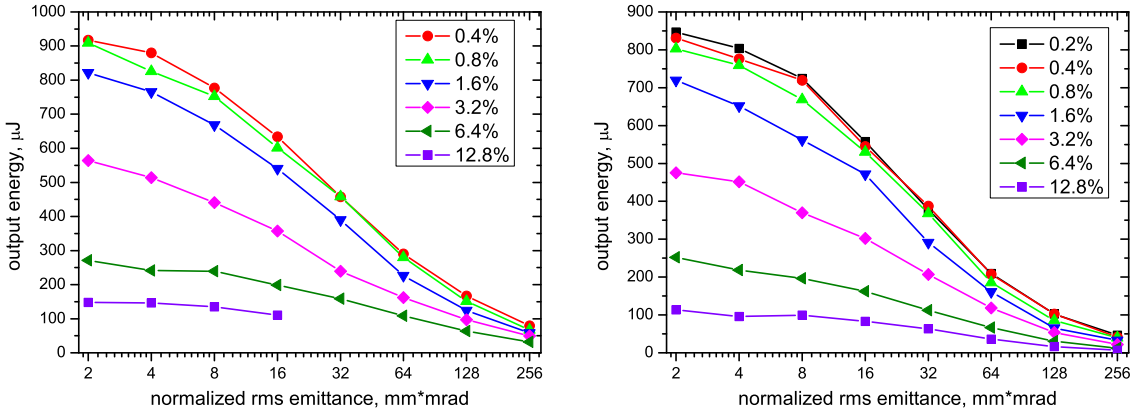

(a) model. 0.3 THz

(b) model. 1.0 THz

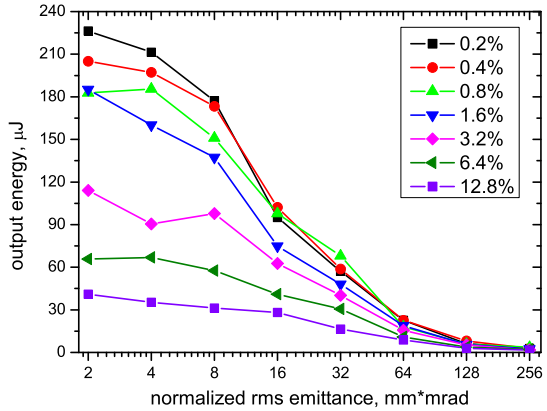

(c) model. 3.0 THz

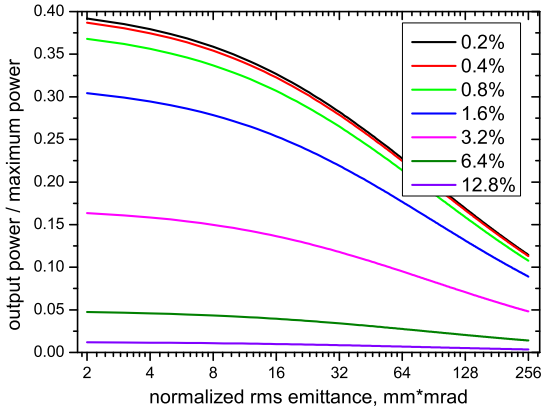

(d) theory. 3.0 THz

Figure 3: (Color online) (a-c) The output energy of the THz pulse calculated as the function of the normalized bunch emittance for different macroparticle relative energy spreads and resonant frequencies. (d) The relative power as the function of the normalized bunch emittance theoretically evaluated for different macroparticle relative energy spreads at the 1.0 THz resonant frequency.

the normalized bunch emittance ϵ_n for different values $\delta = \Delta_E/E_e$, where Δ_E is the macroparticle energy spread and E_e is the mean electron energy in the bunch. The parameters of the simulation are listed in Table 1. The plane-wave resonant frequency of the undulator which is determined as

$$\nu_R = \frac{2c\gamma_0^2}{\lambda_u}\left(1 + K_u^2\right)^{-1}, \tag{23}$$

$$K_u = \frac{eB_u\lambda_u}{\sqrt{8\pi}cm_e}, \quad \gamma_0 = \frac{E_e}{m_e c^2} + 1 \tag{24}$$

is equal to 0.3 THz in this case. As the figure shows, the output pulse energy is extremely sensitive to both the bunch emittance and energy spread. For very low emittance and energy spread (ϵ_n <5 mm·mrad and δ <1%) the model predicts the output energy of up to 1 mJ that corresponds to conversion of more than 10% of the bunch energy. This value is approximately an order of the magnitude higher than typical conversion efficiencies of short-pulse oscillator THz FELs [12, 13]. High conversion efficiency given by the model

for high-quality electron bunch can be explained by the fact that in a super-radiant FEL, electrons lose their energy coherently as long as the bunch duration is less than the half-resonant wavelength. Under these conditions, the loss in electron energy results in a shift of the resonant wavelength to the lower frequency side, the FEL resonance is not broken. This is not true for electron bunches with high energy spread or with high emittance because the difference in electron longitudinal velocities leads to the bunch stretching, incoherent loss of the electron energy, and breaking the FEL resonance condition. The energy drop effect with bunch quality degradation is clear seen in the figure. Thus, E_{THz} <100 μJ when $\epsilon_n > 200$ mm·mrad regardless of the δ values. For $\epsilon_n \approx 20$ mm·mrad, the same E_{THz} values are also predicted when δ >13%.

Table 2: Parameters of simulation. The resonant frequency is 1.0 THz.

Bunch charge, Q_b	1 nC
Mean electron energy, E_e	9.306 MeV
Bunch duration, τ_b	150 fs (rms)
Bunch β_0-function	3.0 m
Magnetic flux density, B_u	0.138 T
Undulator period, λ_u	11 cm
Number of periods, N_u	9
Undulator parameter, K_u	1.0

Energy characteristics of the FEL tuned to the 1.0 THz resonant frequency are shown in Fig. 3b and its parameters are specified in Table 2. The numerical data predict nearly the same level of the peak output energy, $E_{THz} > 0.8$ mJ, as it is for the 0.3 THz resonant frequency. However, the energy dependencies are more sensitive to the bunch quality in this case that is explained by shorter resonant wavelength and more strict requirements to tolerable scatter in electron velocities. Thus, $E_{THz} < 100$ μJ if $\delta > 13\%$ regardless of the ϵ_n values and if $\epsilon_n > 130$ mm·mrad regardless of the δ values.

Table 3: Parameters of simulation. The resonant frequency is 3.0 THz.

Bunch charge, Q_b	0.5 nC
Mean electron energy, E_e	16.46 MeV
Bunch duration, τ_b	100 fs (rms)
Bunch β_0-function	3.0 m
Magnetic flux density, B_u	0.138 T
Undulator period, λ_u	11 cm
Number of periods, N_u	9
Undulator parameter, K_u	1.0

Results of calculation for the resonant frequency of 3.0 THz are shown Fig. 3c. Table 3 lists the calculation parameters. The data are presented for the bunch duration of 100 fs. For the 150 fs bunch duration, calculated THz energy was negligible as far as such bunch length gets close to the resonant half-wavelength. Comparison of Fig. 3a, Fig.

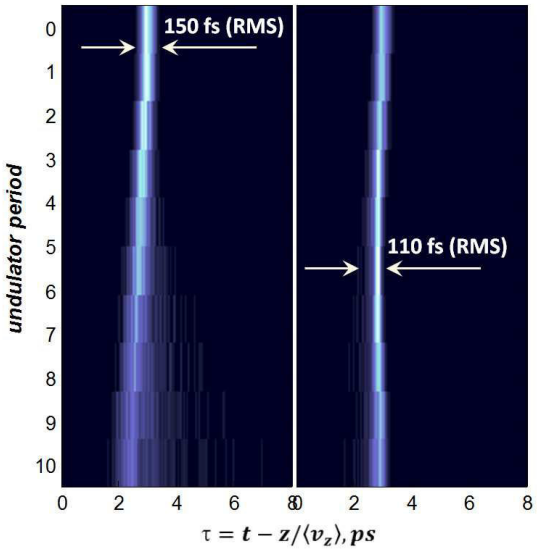

Figure 4: (Color online) The propagation traces of the macroparticles in time frames moving with the electron bunches calculated for $\epsilon_n = 256$ mm·mrad (left graph) and $\epsilon_n = 16$ mm·mrad (right graph) when the resonant frequency was equal to 1.0 THz

3b, and Fig. 3c points to noticeable decrease in the output energy in the last case which does not exceed 0.3 mJ even if FEL is driven by very high-quality electron bunches. For typical values of $\delta = 4\%$ and $\epsilon_n = 100$ mm·mrad, predicted E_{THz} value is only ~ 8 μJ.

It is of interest to compare the numerically calculated data with prediction of the analytical theory of a super-radiant FEL. The details of the theory can be found in Ref. [14] and the results of this prediction are shown in Fig. 3d for the same input parameters as are in Fig. 3b. Comparison between the theoretical and numerical data indicate that the numerical model predicts the FEL output to be more critical to the bunch emittance but less sensitive to the energy spread. Specifically, the numerically calculated output energy drops $\sim$8.2 times whereas the theoretical power does $\sim$2.3 times as the bunch emittance increases from 2 to 128 mm·mrad. When the energy spread increases from 0.2 to 6.4%, the numerical output energy and the theoretical power gain experience the $\sim$3.3 and $\sim$8.3 times drops, respectively.

The discrepancy between the numerical and theoretical data dependencies on the energy spread and bunch emittance can be explained by Fig. 4. The figure shows propagation traces of the macroparticles in a retarded time frame (i.e. in a time frame moving with the electron bunch) which are calculated for two different ϵ_n values. Each horizontal slice of the density plot determines macroparticle position at the beginning of the undulator period. The traces demonstrate that at relatively low emittance, broadening of the electron bunch due nonzero electron energy spread can be suppressed (Fig. 4(b)). Such suppression is directly related to the bunching effect of the generated THz wave which tends to group electrons in such a way that they are pulled into regions near maximum electric field strength. The bunching effect enhances the FEL pulse energy for low bunch emittance. However, it is highly sensitive to the bunch emittance and almost diminishes when the emittance is high enough (Fig. 4(a)).

Fig. 5a shows the pulse energy dependencies as functions of number of the undulator

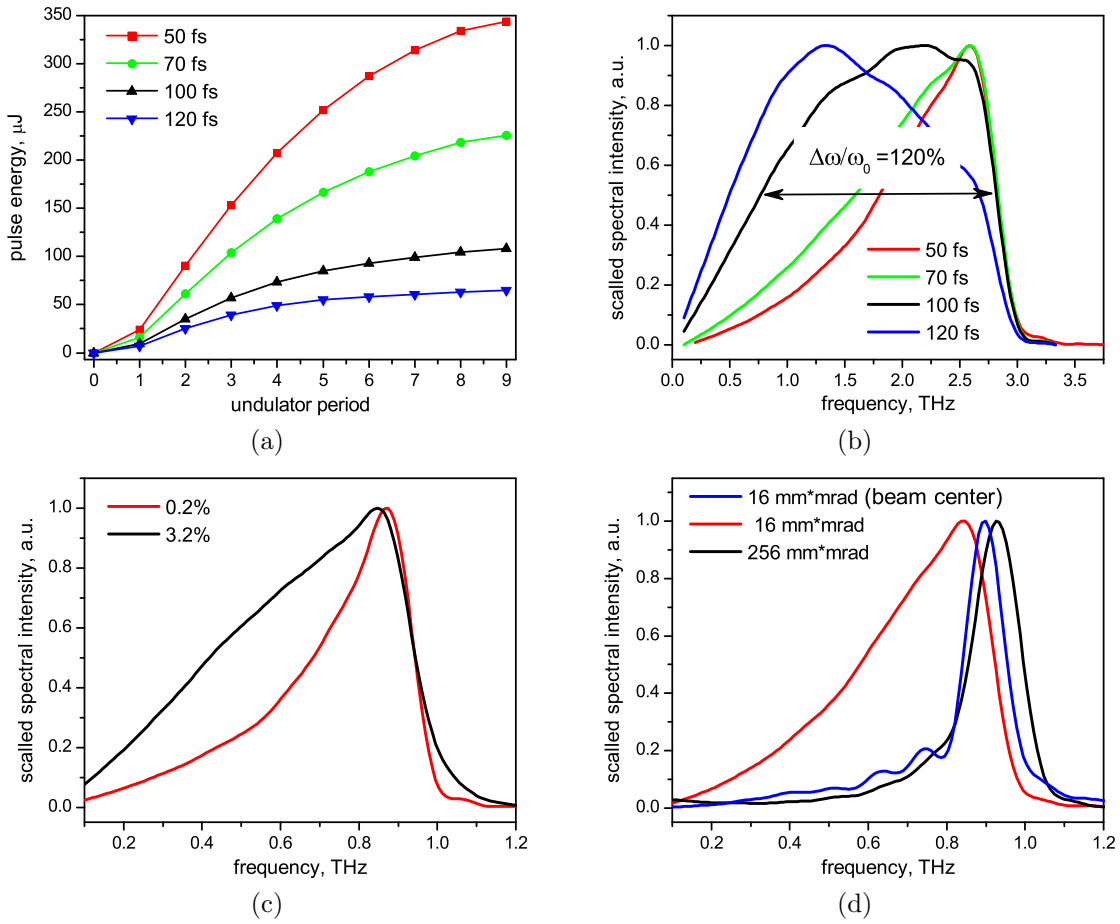

Figure 5: (Color online) (a) The pulse energy vs. the undulator period number calculated for different bunch durations at the resonant frequency of 3.0 THz. (b) The scaled output spectra calculated for different bunch durations at the resonant frequency of 3.0 THz. (c) The scaled output spectra calculated for $\delta = 0.2\%$ and $\delta = 3.2\%$ when $\epsilon_n = 32$ mm·mrad and the resonant frequency $\nu_R = 1$ THz. (d) The scaled output spectra calculated for $\epsilon_n = 16$ mm·mrad and $\epsilon_n = 256$ mm·mrad when $\delta = 1.0\%$ and the resonant frequency $\nu_R = 1$ THz.

periods N_u calculated for different bunch durations at the resonant frequency of 3.0 THz. As is seen, large bunch duration leads to both decrease in slope of the energy dependence and its fast saturation. The data predict more than 5-times drop in the output energy when the bunch duration increases from 0.15 (50 fs) to 0.36 (120 fs) with respect to period of the resonant wavelength (333 fs), respectively.

The normalized spectra of generated pulses calculated for different bunch durations are shown in Fig. 5b. The undulator K_u-parameter is equal to 1.0 for this case, thus the spectra do not exhibit high-order harmonics. As is seen, all the spectral distributions are pulled into the low-frequency side relative to the plane-wave FEL resonant frequency ($\nu_R = 3$ THz) which can be considered as a cut-off frequency. Above this frequency, spectral intensity is close to zero. Causes of the spectral distribution pulling towards low frequencies will be discussed below and here we just mention that an increase in duration of driving electron bunch leads to additional broadening of the spectrum and further low-

frequency shift of its peak intensity. Thus, the relative width of the THz pulse exceeds 100% when the bunch duration approaches to 100 fs. The spectral broadening with increase in bunch duration is due to enhanced contribution of self-amplified spontaneous emission (SASE). Similar spectral broadening is also observed when the electron energy spread grows. In this case, however, intensity peaks doe not shift practically (Fig. 5c).

Spectral transformations due to change in the bunch emittance require more detail discussion. Fig. 5d demonstrates that decrease in the emittance also leads to peak intensity shift to low frequencies. The spectrum gets broader in this case as well, the reason for a cause of such broadening is quite different from the that in Fig. 5b and Fig. 5c. Such behavior becomes more clear if we refer to spatial properties of the generated radiation.

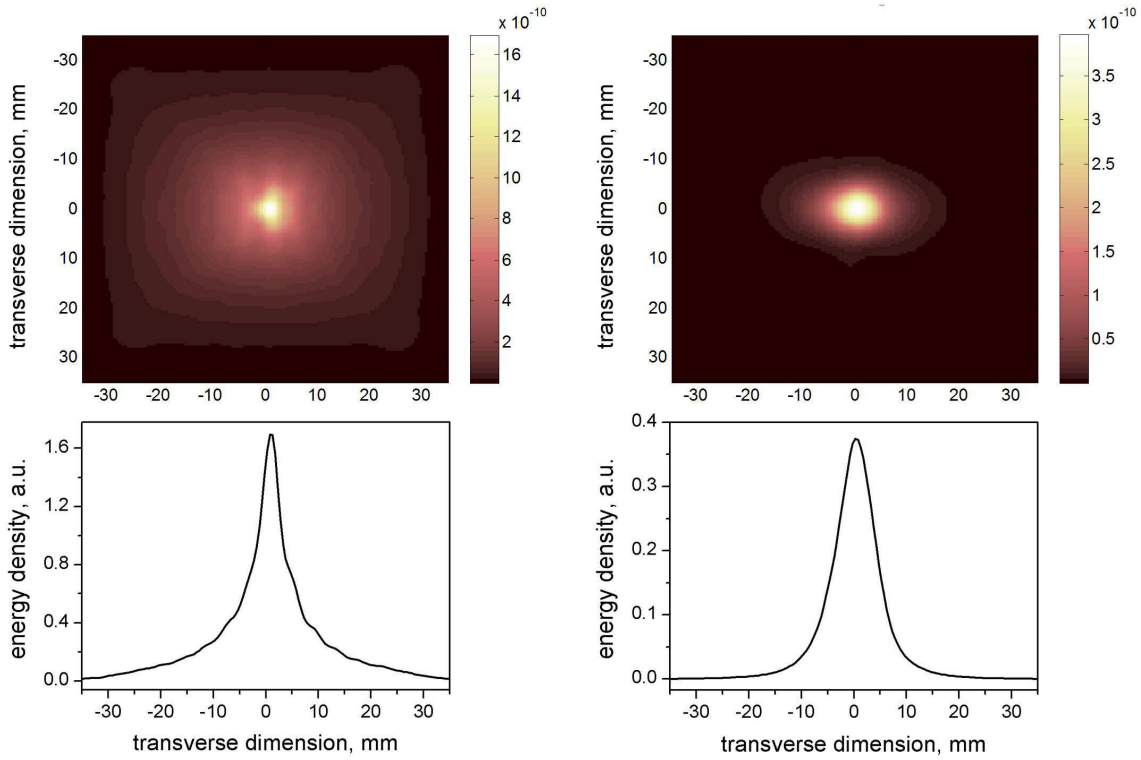

(a) $\epsilon_n = 16$ mm·mrad (b) $\epsilon_n = 256$ mm·mrad

Figure 6: (Color online) Transverse energy density maps and corresponding horizontal intensity profiles of the THz beam at the undulator output calculated for two different ϵ_n values at $\delta = 1.0\%$ and the resonant frequency $\nu_R = 1$ THz

Fig. 6 shows transverse energy density distribution of the THz beam at the undulator output calculated for low and high bunch emittance, respectively. It is seen, that at low emittance, the beam spatial distribution is very broad due to low-intensity halo which fills up the spatial region with more than the 50 cm width. In contrast, at high emittance, generated THz beam is several times less in its spatial width (∼10 mm, FWHM) and its transverse profile is close to the Gaussian.

It is also seen from Fig. 7b that only a few Hermite-Gaussian modes compose the THz beam generated at high ϵ_n values, whereas in the case of low ϵ_n values, the THz beam comprises several hundreds modes (Fig. 7a). A large number of the composing

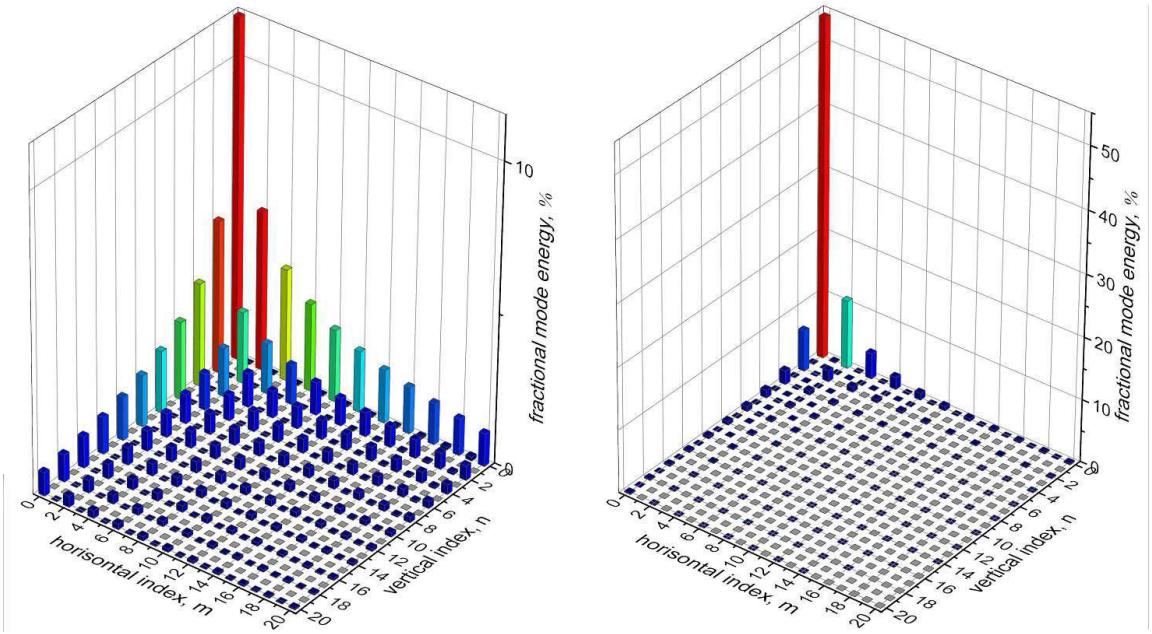

(a) $\epsilon_n = 16$ mm·mrad (b) $\epsilon_n = 256$ mm·mrad

Figure 7: (Color online) The Hermite-Gaussian mode decomposition of the THz beams calculated at $\epsilon_n = 16$ mm·mrad (left graph) and $\epsilon_n = 256$ mm·mrad (right graph) when $\delta = 1.0\%$ and the resonant frequency $\nu_R = 1$ THz.

modes means high angular divergence of the THz beam. The growth in divergence of the THz beam generated by the electron bunch with low emittance is directly related to its small transverse width (see, for instance, Fig. 2a) and to the fact, that the diffraction angle $\alpha_d = c/(\omega w_0)$ of the generated beam is in inverse proportion to width w_0 of the generation region.

The FEL resonant condition for off-axis wave generation is modified with respect to Eq. (23) and takes the form [15]:

$$\nu_{RN} = \frac{2c\gamma_0^2}{\lambda_u}\left(1 + K_u^2 + \gamma_0^2\alpha^2\right)^{-1}, \tag{25}$$

where α is the angle between observation direction and axis of the undulator. (25) indicates decreasing the resonant frequency for off-axis wave generation. Thus, the stronger angular divergence of generated radiation, the larger its spectrum shifts to the low-frequency side and broadened. This is proved by comparison of spectral distributions at $\epsilon_n = 16$ mm·mrad for whole THz beam and for its central part which is confined by the 10×10 mm region (Fig. 5d). As is seen in Fig. 5d, the near-axial spectrum is considerably narrower than the whole beam spectrum and its peak intensity is located closer to the ν_R value.

The FEL spectra shown in Fig. 5b, Fig. 5c, and Fig. 5d have been calculated for the resonant frequencies of 1 and 3 THz when the undulator parameter $K_u = 1$. Under the above conditions, no evident high-order frequency harmonics have been observed in the THz spectra. Fig. 8 shows THz spectra calculated for $\nu_R = 0.3$ THz when $K_u \approx 2.3$ was more than two times higher. The spectra exhibits both odd and even higher-order harmonics. The paraxial spectrum is enriched by odd harmonics. Even harmonics are

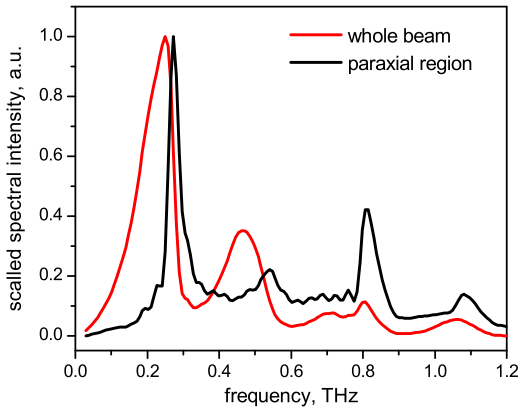

Figure 8: (Color online) The scaled output spectra of whole THz beam and its paraxial region calculated for $\epsilon_n = 16$ mm·mrad and when $\delta = 1.0\%$ and the resonant frequency $\nu_R = 0.3$ THz.

more intensive in spectrum of the whole THz beam. Such results do not contradict the FEL theory [15]. Different harmonics contribution of the spectra considered are due to the fact that axially-generated THz wave exhibits inharmonious time behavior that is symmetrical within the wave period that is not true for off-axis wave.

4 Conclusions

We have considered an open-type super-radiant THz FEL having a simple nontapered undulator with plane magnets. For the 0.99 m long undulator comprising 9 periods of the 11 cm length, we predict output pulse energy of up to $E_{THz} = 1$ mJ in the frequency range of 1.0 - 3.0 THz when FEL is excited by an electron bunch with charge $Q_b = 1$ nC, duration $\tau_b = 150$ fs (rms), normalized emittance $\epsilon_n < 5$ mm·mrad (rms), and energy spread $\delta < 1.0\%$. At the 3 THz operating frequency, we expect up to 0.25 mJ in output pulse energy when $Q_b = 0.5$ nC, $\tau_b = 100$ fs (rms) at the same ϵ_n and δ values. The specified above requirements to ϵ_n and δ are very strict and seem to be hard to realize. For their more realistic values, $\epsilon_n < 100$ mm·mrad and $\delta < 5.0\%$, we predict $E_{out} > 100$ μJ @ 0.3 THz, $E_{out} > 60$ μJ @ 1.0 THz, and $E_{out} > 8$ μJ @ 3.0 THz. Comparison of the results obtained with data of known analytical models indicate that our numerical model predicts the FEL output to be more critical to the bunch emittance but less sensitive to the energy spread. The discrepancy is related to the bunching effect of generated THz field on electrons that enhances the FEL output at low ϵ_n.

We have also analyzed effects of electron bunch parameters on spectral and spatial properties of the THz radiation and shown that increase in the bunch duration and electron energy spread leads to broadening of the THz spectrum. The cause of such spectral broadening is enhanced contribution of self-amplified spontaneous emission (SASE). For the considered interaction geometry, we have also predicted spectral broadening and degradation in angular divergence of the generated radiation with improve in spatial quality (decrease in the emittance) of the electron bunch. Both the predicted properties of the FEL have been shown to be directly related to diffraction effects and FEL resonance condition for nonaxial light generation.

R.C. acknowledges Dr. V. Ziemann and Dr. M. Hamberg for helpful discussions. He also acknowledges Prof. M. Larsson and Stockholm-Uppsala FEL Centre for the encouraging and support.

References

[1] Y. Pinhasi, V. Shterngartz, and A. Gover, Phys. Rev. E **54**, 6774 (1996).

[2] Y. Pinhasi, Yu. Lurie, and A. Yahalom, Nucl. Instrum. Methods Phys. Res., Sect. A **475**, 147 (2001).

[3] M. J. de Loos, C. A. J. van der Geer, S. B. van der Geer, A. F. G. van der Meer, D. Oepts, and R. Wünsch, Nucl. Instrum. Methods Phys. Res., Sect. A **507**, 97 (2003).

[4] V. Zhaunerchyk, R. T. Jongma, Yu. Lurie, Y. Pinhasi, and W. J. van der Zande, Appl. Phys. Lett. **97**, 231109 (2010).

[5] V. Zhaunerchyk *et al.*, Phys. Rev. Spec. Top. Accel. Beams **15**, 050701 (2012).

[6] W. M. Sharp, E. T. Scharlemann, and W. M. Fawley, Nucl. Instr. Meth. Phys. Res. A **296**, 335 (1990).

[7] V. Goryashko, private communications.

[8] V. A. Papadichev, O. A. Smith, Nucl. Instr. Meth. Phys. Res. A **483**, 367 (2002).

[9] J. Buon, Beam Phase Space and Emittance, Paris-11 Univ. Lab. de l'Accelerateur Lineaire: Technical report (1990).

[10] D. A. Edwards, M. J. Syphers, An Introduction to the Physics of High Energy Accelerators, Wiley (1993).

[11] G. Mishra, V. Gupta, N. P. Rajput, B. Kuske, D. Kraemer, R. Bakker, Nucl. Instr. Meth. Phys. Res. A **527**, 233 (2004).

[12] V. Zhaunerchyk *et al.*, Phys. Rev. Spec. Top. Accel. Beams **15**, 050701 (2012).

[13] R. Chulkov, V. Goryashko, D. Arslanov, R. T. Jongmac, W. J. van der Zandec, and V. Zhaunerchyk, Phys. Rev. Spec. Top. Accel. Beams, submitted for publication (2014).

[14] 4GLS Conceptual Design Report, Chapters 4, 8. (*http*: *//www.4gls.ac.uk/cdr/ 4GLS$_C$DR.PartAonline.pdf*).

[15] G. Dattoli, A. Renieri, A. Torre, Lectures on the Free Electron Laser Theory and Related Topics, World Scientific, 637 pages (1993).